Modelling how the altered usage of cell entry pathways by the SARS-CoV-2 Omicron variant may affect the efficacy and synergy of TMPRSS2 and Cathepsin B/L inhibitors

Pranesh Padmanabhan[1,*], Narendra M. Dixit[2,3,*]

[1]Clem Jones Centre for Ageing Dementia Research, Queensland Brain Institute, The University of Queensland, Brisbane, Australia 4072

[2]Department of Chemical Engineering, Indian Institute of Science, Bangalore, India 560012

[3]Centre for Biosystems Science and Engineering, Indian Institute of Science, Bangalore, India 560012

[*]**Correspondence:**

Pranesh Padmanabhan, Narendra M. Dixit

Email: p.padmanabhan@uq.edu.au; narendra@iisc.ac.in

Manuscript details:

Abstract: 150 words; Main Text: ~5000 words; Figures: 5; Tables: 1; References: 47

ABSTRACT

The SARS-CoV-2 Omicron variant harbours mutations in its spike protein, which may affect its cell entry, tropism, and response to interventions. To elucidate these effects, we developed a mathematical model of SARS-CoV-2 entry into cells and applied it to analyse recent *in vitro* data. SARS-CoV-2 enters cells using host proteases, either Cathepsin B/L or TMPRSS2. We estimated >4-fold increase and >3-fold decrease in entry efficiency using Cathepsin B/L and TMPRSS2, respectively, of the Omicron variant relative to the original or other strains in a cell type-dependent manner. Our model predicted that Cathepsin B/L inhibitors would be more and TMPRSS2 inhibitors less efficacious against the Omicron than the original strain. Furthermore, the two inhibitor classes would exhibit synergy, although the drug concentrations maximizing synergy would have to be tailored to the Omicron variant. These findings provide insights into the cell entry mechanisms of the Omicron variant and have implications for interventions.

Keywords: SARS-CoV-2; COVID-19; Omicron; Spike protein; TMPRSS2; Cathepsin; Mathematical modelling; Viral kinetics; Drug synergy

INTRODUCTION

The SARS-CoV-2 variant Omicron, declared a variant of concern on 25th November 2021, has become the dominant strain worldwide. It harbours as many as 37 mutations in the spike protein compared to the original SARS-CoV-2 strain (Cameroni et al., 2021) and is able to evade neutralising antibodies generated by previously infected or vaccinated individuals (Cameroni et al., 2021; Garcia-Beltran et al., 2021; Hoffmann and et al, 2021; Willett et al., 2022), possibly leading to its increased transmissibility and rapid global spread. The spike protein facilitates the entry of the virus into cells (Hoffmann et al., 2020a; Koch et al., 2021). Indeed, emerging data indicates that the high number of mutations in the Omicron variant affects its viral entry properties and cell tropism (Garcia-Beltran et al., 2021; Hoffmann and et al, 2021; Meng et al., 2021; Peacock et al., 2022; Willett et al., 2022; Zhao et al., 2021), which in turn may influence its ability to establish infection post-exposure and the severity of the subsequent symptoms. How the mutations influence entry and the efficacies of entry inhibitors remains to be elucidated.

Early studies showed that the original SARS-CoV-2 (Wuhan-Hu-1) strain displayed broad cell tropism, with viral entry a key determinant of the tropism both *in vitro* (Hoffmann et al., 2020a) and *in vivo* (Liu et al., 2021). Intriguingly, multiple recent *in vitro* studies suggest that cell tropism of the Omicron variant may be altered and its entry efficiency may be different from the original and other variants in a cell line-dependent manner (Garcia-Beltran et al., 2021; Hoffmann and et al, 2021; Meng et al., 2021; Peacock et al., 2022; Zhao et al., 2021). For instance, SARS-CoV-2 pseudotyped virus bearing either the B.1 or the Delta variant spike protein showed higher entry efficiency than the Omicron pseudotyped virus in Caco-2 (human, colon) and Calu-3 (human, lung) cells, whereas the Omicron pseudotyped virus entered Vero (African green monkey, kidney) and 293T (human, kidney) cells more efficiently than the other variants(Hoffmann and et al, 2021). Similar trends were observed in live SARS-CoV-2 virus

infection assays (Meng et al., 2021; Zhao et al., 2021): the Delta variant infection spread was significantly greater than the Omicron variant in Calu-3 cells (Meng et al., 2021; Zhao et al., 2021), whereas the spread of the two variants was similar in VeroE6 cells (Zhao et al., 2021). What causes the entry efficiency of the Omicron variant relative to other variants to be higher in some cells and lower in others?

The first step in SARS-CoV-2 entry into target cells is the binding of the viral spike protein, S, with the host cell surface receptor angiotensin-converting enzyme 2 (ACE2) (Balistreri et al., 2021; Jackson et al., 2022). Cell tropism is thus expected to be affected by ACE2 expression levels (Hoffmann et al., 2020a; Koch et al., 2021; Liu et al., 2021). The Omicron spike protein binds soluble human ACE2 strongly (Cameroni et al., 2021; Hoffmann and et al, 2021). Further, ACE2 is necessary for the entry of all SARS-CoV-2 variants (Garcia-Beltran et al., 2021; Hoffmann and et al, 2021; Hoffmann et al., 2020a; Meng et al., 2021; Zhao et al., 2021). Thus, any variation in ACE2 expression across cell types is likely to have similar effects on the entry efficiencies of all the variants. The cell type-dependent variation in the entry efficiency of the Omicron variant is therefore unlikely to arise from the variations in the ACE2 expression level across cell types. Omicron spike protein incorporation into pseudotyped virus appears to be compromised compared to the Delta and Wuhan D614G strains (Meng et al., 2021). However, this reduction in spike protein density is expected to decrease the Omicron entry efficiency across all cell types, thus ruling it out as a potential cause of the differential entry efficiency observed.

Following ACE2 engagement, successful entry requires that the spike protein be cleaved into subunits by host proteases, either by the transmembrane serine protease TMPRSS2 at the plasma membrane or the cysteine proteases Cathepsin B and Cathepsin L in the endosomal vesicles (Jackson et al., 2022). The proteases TMPRSS2 and Cathepsin B/L are thought to work independently, facilitating SARS-CoV-2 entry through two independent

pathways (Koch et al., 2021; Padmanabhan et al., 2020) (Fig. 1A). We recently analysed data on SARS-CoV-2 pseudotyped virus infection *in vitro* (Hoffmann et al., 2020a) using a mathematical model of SARS-CoV-2 entry and found that the relative usage of the TMPRSS2 and Cathepsin B/L entry pathways by the original SARS-CoV-2 strain varied widely across cell lines (Padmanabhan et al., 2020). For example, Vero cells predominantly admitted entry through the Cathepsin B/L pathway, whereas Calu-3 cells allowed entry via the TMPRSS2 pathway. Vero cells overexpressing TMPRSS2 permitted entry via both pathways (Hoffmann et al., 2020a). Importantly, the original strain displayed the ability to use either pathway, with the preferred pathway possibly based on the relative expression levels of the two proteases (Koch et al., 2021). We reasoned that the Omicron variant might use these pathways differently from the original (or the Delta) strain, possibly underlying its differential entry efficiency and altered cell tropism.

Here, to elucidate the entry mechanisms of the Omicron variant, we developed a mathematical model of SARS-CoV-2 entry that explicitly considered the two independent entry pathways. Applying the model to the analysis of available *in vitro* data, we deduced the usage of the two pathways by the Omicron variant relative to the other strains. We then applied the model to predict the efficacies of drugs that target host proteases facilitating entry via the two pathways.

METHODS

Model of SARS-CoV-2 entry and the efficacy of entry inhibitors targeting host proteases

In vitro experiments typically employ virions or pseudotyped viral particles bearing the spike protein, S, of a specific SARS-CoV-2 strain to assess its entry efficiency, determined by measuring the fraction of cells infected post virus exposure. We previously developed a mathematical model to analyse such experiments (Padmanabhan et al., 2020). We adapted the

model here to compare the pathway usage of the Omicron variant relative to other variants and to predict the effect of entry inhibitors.

In culture, the expression levels of host proteases are expected to vary across cells and affect viral entry into the cells. We let the expression levels, n_t and n_c, of TMPRSS2 and Cathepsin B/L, respectively, follow the log-normal distributions $\psi_t(n_t)=\frac{1}{n_t\sigma_t\sqrt{2\pi}}e^{-\frac{(\ln n_t-\overline{n_t})^2}{2\sigma_t^2}}$ and $\psi_c(n_c)=\frac{1}{n_c\sigma_c\sqrt{2\pi}}e^{-\frac{(\ln n_c-\overline{n_c})^2}{2\sigma_c^2}}$, with $\overline{n_t}$ and $\overline{n_c}$ the associated means, and σ_t and σ_c the standard deviations. Thus, at the start of infection, a fraction $\phi_{tc}=\psi_t(n_t)\psi_c(n_c)\Delta n_t\Delta n_c$, of the cells in culture would express proteases in the narrow range Δn_t and Δn_c around n_t and n_c, respectively. Recognizing that entry efficiency would increase with protease expression (Padmanabhan et al., 2020; Padmanabhan and Dixit, 2011, 2012), we defined the relative susceptibility of these latter cells to virus entry through the TMPRSS2 pathway, S_t, and the Cathepsin B/L pathway, S_c, as $S_t=\frac{(n_t)^{h_t}}{(n_t^{50})^{h_t}+(n_t)^{h_t}}$ and $S_c=\frac{(n_c)^{h_c}}{(n_c^{50})^{h_c}+(n_c)^{h_c}}$, where h_t and h_c were Hill coefficients, and n_t^{50} and n_c^{50} were expression levels at which $S_t=0.5$ and $S_c=0.5$, respectively. The overall susceptibility of the cells was thus $S_{tc}=S_t+S_c-S_tS_c$, based on the independence of the two pathways.

We defined T_{tc} as the above subpopulation (or fraction) of cells and considered a total of $M\times N$ such subpopulations, with $t=1,\ 2,..,M$ and $c=1,\ 2,..,N$, defining the range of expression levels of the two proteases across cells. The following equations then described the ensuing viral dynamics:

$$\frac{dT_{tc}}{dt} = (\lambda - \mu)T_{tc} - kS_{tc}T_{tc}V; \quad t = 1,2,...,M; \quad c = 1,2,...,N \tag{1}$$

$$\frac{dI_{tc}}{dt} = kS_{tc}T_{tc}V - \delta I_{tc}; \quad t = 1,2,...,M; \quad c = 1,2,...,N \tag{2}$$

$$\frac{dV}{dt} = p\sum_{c=1}^{N}\sum_{t=1}^{M} I_{tc} - c_V V \tag{3}$$

Here, cells in the subpopulation T_{tc} proliferate and die with rate constants λ and μ, respectively, and get infected by free virions, V, with the second order rate constant kS_{tc}. k is thus the rate constant of the infection of the subpopulation for which entry is not limited by the proteases, *i.e.*, for cells with $S_{tc} = 1$. Infection produces corresponding infected cell subpopulations I_{tc}, which release free virions at the rate p per cell and die with a rate constant δ. Virions are cleared with the rate constant c_V. With pseudotyped viruses, which are replication incompetent, we let $p = 0$.

In the presence of a TMPRSS2 inhibitor, a Cathepsin B/L inhibitor, or both, the susceptibilities were lowered to $S_{tc}(D_T)$, $S_{tc}(D_C)$, and $S_{tc}(D_T, D_C)$, respectively, where D_T and D_C were the concentrations of the TMPRSS2 and Cathepsin B/L inhibitors. We describe the latter susceptibilities below.

Effect of host protease inhibitors. In the presence of a protease inhibitor targeting a specific protease, the drug would bind and block a fraction of the protease molecules from facilitating entry. With a TMPRSS2 inhibitor at concentration D_T, we described the abundance of free TMPRSS2, denoted n_t^f, using $n_t^f = \frac{\gamma_T}{\gamma_T + D_T} n_t$, where γ_T was the drug concentration that reduced the abundance by half. The expression for n_t^f could be derived mechanistically assuming reaction equilibrium of drug-protease binding and species balance constraints

(Padmanabhan et al., 2020; Padmanabhan and Dixit, 2011). The susceptibility of cells T_{tc} to infection through the TMPRSS2 pathway thus reduced to $S_t(D_T) = \frac{(n_t^f)^{h_t}}{(n_t^{50})^{h_t} + (n_t^f)^{h_t}}$. We assumed that the susceptibility through the Cathepsin B/L pathway was unaffected by a TMPRSS2 inhibitor. Similarly, in the presence of a Cathepsin B/L inhibitor at concentration D_C, we let the abundance of free Cathepsin B/L, n_c^f, follow $n_c^f = \frac{\gamma_C}{\gamma_C + D_C} n_c$, and the susceptibility through the Cathepsin B/L pathway be reduced to $S_c(D_C) = \frac{(n_c^f)^{h_c}}{(n_c^{50})^{h_c} + (n_c^f)^{h_c}}$. When both types of inhibitors are used simultaneously, the susceptibility was $S_{tc}(D_T, D_C) = S_t(D_T) + S_c(D_C) - S_t(D_T) S_c(D_C)$.

To assess whether the drugs exhibited synergy, we predicted the population of infected cells in the absence of drugs, I_{tc}, in the presence of a TMPRSS2 inhibitor, $I_{tc}(D_T)$, a Cathepsin B/L inhibitor, $I_{tc}(D_C)$, and both, $I_{tc}(D_T, D_C)$, at any given time following the start of infection. The total fractions of cells unaffected by the drugs individually and together were then given by $f^u(D_T) = \frac{\sum_{c=1}^{N}\sum_{t=1}^{M} I_{tc}(D_T)}{\sum_{c=1}^{N}\sum_{t=1}^{M} I_{tc}}$, $f^u(D_C) = \frac{\sum_{c=1}^{N}\sum_{t=1}^{M} I_{tc}(D_C)}{\sum_{c=1}^{N}\sum_{t=1}^{M} I_{tc}}$, and $f^u(D_T, D_C) = \frac{\sum_{c=1}^{N}\sum_{t=1}^{M} I_{tc}(D_T, D_C)}{\sum_{c=1}^{N}\sum_{t=1}^{M} I_{tc}}$.

We computed the expected fraction of cells unaffected by drugs assuming Bliss independence using $f^u_{Bliss}(D_T, D_C) = f^u(D_T) f^u(D_C)$. The extent of Bliss synergy then followed as $\beta_{Bliss} = f^u_{Bliss}(D_T, D_C) - f^u(D_T, D_C)$, so that

$$\beta_{Bliss} = \frac{\sum_{c=1}^{N}\sum_{t=1}^{M} I_{tc}(D_T)}{\sum_{c=1}^{N}\sum_{t=1}^{M} I_{tc}} \times \frac{\sum_{c=1}^{N}\sum_{t=1}^{M} I_{tc}(D_C)}{\sum_{c=1}^{N}\sum_{t=1}^{M} I_{tc}} - \frac{\sum_{c=1}^{N}\sum_{t=1}^{M} I_{tc}(D_T, D_C)}{\sum_{c=1}^{N}\sum_{t=1}^{M} I_{tc}} \quad (4)$$

Mean-field model to compare entry efficiencies of variants

To quantify the relative efficiency of the usage of the Cathepsin B/L and TMPRSS2 pathways by the Omicron variant, we developed a mean-field version of the model above by considering 'average' susceptibilities of the cells to entry via the two pathways. We thus let target cells, T, be infected by pseudotyped virions, V, to produce infected cells, I, depending on the 'mean' expression levels of TMPRSS2 and Cathepsin B/L. The following equations then described the ensuing dynamics:

$$\frac{dT}{dt} = (\lambda - \mu)T - k\overline{S_{tc}}TV \quad (5)$$

$$\frac{dI}{dt} = k\overline{S_{tc}}TV - \delta I \quad (6)$$

$$\frac{dV}{dt} = pI - c_V V \quad (7)$$

Here, we defined the average susceptibility of the cell population to entry via the Cathepsin B/L pathway as $\overline{S_c}$ and that via the TMPRSS2 pathway as $\overline{S_t}$. These susceptibilities increase with the expression levels of the respective proteases and saturate to unity when the levels are in excess. For a given cell type, a viral variant that has a higher $\overline{S_c}$ (or $\overline{S_t}$) would be more efficient at entry via the Cathepsin B/L (or TMPRSS2) pathway than a variant with a lower $\overline{S_c}$ (or $\overline{S_t}$). Assuming entry via the two pathways to be independent, the overall susceptibility of the population to entry can be written as $\overline{S_{tc}} = \overline{S_t} + \overline{S_c} - \overline{S_t}\,\overline{S_c}$. This susceptibility determined the rate of target cell infection relative to the maximal rate k. We let $p = 0$ as described above.

Data analysis using the mean-field model. Experiments with pseudotyped virions typically last less than 24 h. It is reasonable to assume that cell proliferation and death do not affect the infection dynamics significantly during this period. Therefore, we ignored the proliferation and death terms in Eqs. (5-6), which allowed us to derive an analytical expression for the time

193 evolution of the population of infected cells: $I(t) = T_0\left(1 - e^{\frac{k\overline{S_{tc}}V_0}{c_V}(e^{-c_V t}-1)}\right)$, where T_0 and

194 V_0 are the initial target cell density and viral concentration, respectively. Using this expression,

195 we obtained the fraction of cells infected by the pseudotyped virions, χ, at time t_d post-

196 infection as

197 $$\chi = \frac{I(t_d)}{T_0} = \left(1 - e^{\vartheta\overline{S_{tc}}V_0}\right) \quad (8)$$

198 where $\vartheta = \frac{k}{c_V}(e^{-c_V t_d} - 1)$ is a constant for a given t_d.

199 We fit this expression to measured data from recent assays and estimated the efficiency

200 of the usage of the two pathways by the Omicron variant relative to the original or other strains.

201

202 **Model parameters.** We chose model parameters, such as the target cell proliferation and death

203 rate constants, from the literature (Gonçalves et al., 2020; Hoffmann et al., 2020a; Jiang et al.,

204 2019; Padmanabhan and Dixit, 2015; Ursache et al., 2015) and our previous study

205 (Padmanabhan et al., 2020). The model parameter values and initial conditions are summarised

206 in Table 1.

207

208 **RESULTS**

209 **Correlation of entry efficiency with pathway usage**

210 To test our hypothesis that the Omicron variant uses the entry pathways differently, we

211 examined data from the recent experiments of Hoffmann et al. (2021), who measured the extent

212 of infection of cells *in vitro* by the Omicron variant (BA.1 sublineage) relative to other variants

213 in different cell types. Interestingly, we found a correlation between the entry efficiency of the

214 Omicron variant and the relative usage of the two entry pathways by the original strain (Fig.

215 1B). With cell lines (Calu-3 and Caco-2) where the usage of the TMPRSS2 entry pathway by

216 the original strain was dominant, the Omicron pseudotyped virus entry was significantly less

efficient than the B.1 and delta strains. By contrast, the Omicron virus entry was more efficient in cell lines (293T and Vero) where the Cathepsin B/L entry pathway usage by the original strain was dominant (Fig. 1B). One possible interpretation of this relationship is that the Omicron variant entry is relatively less efficient through the TMPRSS2 pathway and more efficient via the Cathepsin B/L pathway than the other strains. Consistent with this notion, camostat mesylate, a TMPRSS2 inhibitor, was less potent against the Omicron variant than the Delta variant in blocking live virus infection of VeroE6 cells overexpressing TMPRSS2, which allows entry via both pathways (Zhao et al., 2021). Moreover, syncytium formation in a cell-cell fusion assay, which requires TMPRSS2 but not Cathepsins, was severely impaired for the Omicron variant compared to both the Delta (Meng et al., 2021; Zhao et al., 2021) and the Wuhan-Hu-1 D614G (Meng et al., 2021) strains. The increased efficiency of Cathepsin B/L usage together with the reduced efficiency of TMPRSS2 usage by the Omicron variant may explain its altered cell tropism relative to the original strain or other variants.

Omicron variant entry with low Cathepsin B/L expression

We reasoned that the increased efficiency of Cathepsin B/L usage and reduced TMPRSS2 usage by the Omicron variant would imply that the variant would successfully enter cells that express low Cathepsin B/L levels, where the original strain might fail. To elucidate this, we performed calculations using our model (Eqs. (1-3)) by varying the expression level of Cathepsin B/L. We first set n_t^{50}=3.6 x 10^5 copies/cell and n_c^{50}=8 x 10^4 copies/cell for the Omicron variant and n_t^{50}=1.2 x 10^5 copies/cell and n_c^{50}=2.4 x 10^5 copies/cell for the original strain so that for given distributions of the TMPRSS2 and Cathepsin B/L expression levels, the susceptibility of cells to entry via the TMPRSS2 pathway was lower (Fig. 2A) and the Cathepsin B/L pathway was higher (Fig. 2B) for the Omicron variant than the original strain. Recall that n_t^{50} is the expression level at which entry efficiency via the TMPRSS2 pathway is

half-maximal. Thus, the lower the n_t^{50}, the more efficient is the usage of the TMPRSS2 pathway. Analogous notions apply to the Cathepsin B/L pathway. We then considered three *in silico* cell lines with a constant TMPRSS2 distribution (Fig. 2C) but different Cathepsin B/L levels, the latter termed low, medium and high (Fig. 2D). For each of these cell lines, we predicted the distributions of cells infected by the original strain as well as by the Omicron variant (Fig. 2E) and compared the two (Fig. 2F). We found that when Cathepsin B/L expression was high, the advantage of the Omicron variant was undermined because of the abundance of Cathepsin B/L, so that the two strains had similar entry levels (Fig. 2F). As the expression level decreased, the Omicron variant was more successful at entry. With medium expression level, the Omicron variant had ~1.4-fold greater entry, and with low expression level, it had more than ~2.9-fold greater entry success than the original strain.

With these predictions further strengthening our hypothesis above, we asked whether we could apply our model to analyse available data to quantify the increased (decreased) entry efficiency of the Omicron variant via the Cathepsin B/L (TMPRSS2) pathway. Because the distributions of the protease levels across cells are not known, we employed a simplified, mean-field version of our model for this analysis (Methods).

Quantitative estimates of relative entry efficiency

We considered data from cell types where the original strain nearly exclusively entered via either the Cathepsin B/L or the TMPRSS2 pathways, so that we could estimate the relative efficiency of the usage of either pathway by the Omicron variant. We thus examined first data from Garcia-Beltran et al. (2021), who measured the fraction of 293T-ACE2 cells infected by pseudotyped virus bearing the wild-type or the Omicron spike proteins at different viral concentrations, V_0 (Fig. 3A). 293T-ACE2 cells predominantly permit original strain entry via the Cathepsin B/L pathway (Padmanabhan et al., 2020). Given the relatively poor efficiency

of TMPRSS2 usage by the Omicron variant, we made the approximation $\overline{S_{tc}} \approx \overline{S_c}$ in Eqs. (5-6). Using the resulting expression (Eq. (8)), we fit predictions of χ as a function of V_0 to the corresponding experimental data (Garcia-Beltran et al., 2021) and estimated the composite parameter $\vartheta\overline{S_c}$ for the wild-type (wt) and the Omicron variant. Our model provided good fits to the data (Fig. 3A). Taking ratios of the estimated composite parameter and recognizing that ϑ is unlikely to be strain dependent, we obtained $\overline{S_c^{Omicron}}/\overline{S_c^{wt}}\sim 4.6$, indicating an ~4.6-fold increased efficiency of the usage of the Cathepsin B/L pathway by the Omicron variant in 293T-ACE2 cells relative to the original strain.

We next analysed the experiments of Hoffmann et al. (2021) mentioned above (Fig 1B). We focussed on Calu-3 cells, which appear to allow entry of the original strain nearly exclusively via TMPRSS2. Here, we therefore made the approximation $\overline{S_{tc}} \approx \overline{S_t}$ in Eqs. (5-6). Unlike the above dataset, measurements here were available at a single initial viral load. Further, measurements were available of the fractions of cells infected by viruses pseudotyped with the Omicron variant relative to those with the B.1 or Delta variants. Note that B.1 has spike proteins identical to the original strain except for the D614G mutation. Because the overall infection of Calu-3 cells is small, Taylor series expansion of Eq. (7) yielded the approximation $\chi \approx \vartheta\overline{S_t}V_0$. Accordingly, the susceptibility of cells to entry via the TMPRSS2 pathway of the Omicron variant relative to the B.1 strain would be given by the ratio of the fractions of cells infected in the two assays: $\overline{S_t^{Omicron}}/\overline{S_t^{B.1}} = \chi^{Omicron}/\chi^{B.1}$. Using the latter expression and the corresponding data yielded $\overline{S_t^{Omicron}}/\overline{S_t^{B.1}}\sim 0.28$ and $\overline{S_t^{Omicron}}/\overline{S_t^{Delta}}\sim 0.12$. Thus, we estimated ~3.6-fold and ~8.3-fold decreased efficiency of the Omicron variant in using TMPRSS2 for entry in Calu-3 cells compared to the B.1 and Delta strains, respectively (Fig. 3B).

Together, thus, the Omicron variant appears to have evolved to use Cathepsin B/L more efficiently and TMPRSS2 less efficiently for virus entry than the original and other strains.

Efficacies of Cathepsin B/L and TMPRSS2 inhibitors in blocking Omicron variant entry

Drugs targeting the proteases Cathepsin B/L and TMPRSS2 offer promising routes to treat SARS-CoV-2 infection (Hashimoto et al., 2021; Hoffmann et al., 2020a; Hoffmann et al., 2020b; Kreutzberger et al., 2021; Ou et al., 2021). The improved efficiency of Cathepsin B/L usage and reduced efficiency of TMPRSS2 usage would imply that drugs targeting the former but not the latter would be preferred for treating infections with the Omicron variant. To examine this, we applied our model (Eqs. (1-3)) to predict the ability of the two classes of inhibitors to prevent viral entry. We considered an *in silico* cell line with log-normal distributions of the expression levels of TMPRSS2 and Cathepsin B/L (Fig. 4A) and the strain-dependent susceptibility of cells to entry via the two pathways (Fig. 2A, B). In the presence of a TMPRSS2 inhibitor, our model predicted that entry of the original strain would decrease in a dose-dependent manner and saturate, for the parameters chosen, to ~45% of that in the absence of the drug (Fig. 4B). The latter plateau represented the entry via the Cathepsin B/L pathway when entry via the TMPRSS2 pathway was fully blocked. Under the same conditions, entry of the Omicron variant saw hardly any decrease compared to that in the absence of the drug. This is because the Omicron variant entry proceeded only minimally via the TMPRSS2 pathway, leaving little room for the drug to act.

The use of a Cathepsin B/L inhibitor, however, had the opposite effect. The entry of the original strain showed hardly any reduction with increase in drug concentration (Fig. 4C). On the other hand, the entry of the Omicron variant decreased in a dose-dependent manner and plateaued to a value of ~38% of that in the absence of the drug.

314 It followed, thus, that Cathepsin B/L inhibitors would be more effective in blocking
315 Omicron variant entry than TMPRSS2 inhibitors.
316
317 **Synergy between Cathepsin B/L and TMPRSS2 inhibitors against both the original strain**
318 **and Omicron variant**
319 Previously, we predicted synergy between the two types of inhibitors in blocking virus
320 entry, which has since been observed in experiments with the original strain (Hoffmann et al.,
321 2020a; Kreutzberger et al., 2021). Here, we applied our model to estimate the extent of synergy
322 with the Omicron variant relative to the original strain (Eqs. (1-4)) (Fig. 5A-J). Given the
323 substantial cell-type dependence in entry efficiency, we first considered two *in silico* cell types,
324 one with relatively low (Fig. 5A) and the other with relatively high (Fig. 5E) mean TMPRSS2
325 expression levels. Both the cell types expressed moderate Cathepsin B/L levels (Fig. 5A, E).
326 The TMPRSS2 and Cathepsin B/L inhibitors worked synergistically to block original strain
327 and Omicron variant entry in a dose-dependent manner, albeit to different extents (Fig. 5B-D,
328 F-H).
329 At low drug levels, Bliss synergy, β_{Bliss}, was minimal because the chances of the drugs
330 acting together on the same cell were minimal (Fig. 5D, H). As the drug levels increased, the
331 synergy increased and plateaued at a value that depended on the expression levels of the
332 proteases and the viral strain (Fig. 5D, H). This effect could be understood by considering the
333 relative usage of the two entry pathways. In our calculations, drug synergy was high when the
334 relative preferences for the two pathways were similar, so that both pathways had to be blocked
335 and drugs targeting both pathways would thus synergize. When usage of either of the two
336 pathways dominated, the drug that blocked the dominant pathway alone had a role, leaving
337 little room for synergy. For instance, when TMPRSS2 levels were low (Fig. 5A), the original
338 strain used both pathways for entry (Fig. 5B), whereas the Omicron variant predominantly used

the Cathepsin B/L pathway. Consequently, the maximum synergy achieved against the original strain (β_{Bliss} = 0.34) was higher than the Omicron variant (β_{Bliss} = 0.07) (Fig. 5B). In contrast, when TMPRSS2 levels were high (Fig. 5E), the original strain predominantly used the TMPRSS2 pathway, and the Omicron variant used both the pathways for entry. The synergy for the Omicron variant (β_{Bliss} = 0.54) was now much higher than that for the original strain (β_{Bliss} = 0.38) (Fig. 5H).

We next predicted synergy by varying either the mean expression levels of TMPRSS2 (Fig. 5I) or Cathepsin B/L (Fig. 5J). The synergy with the original strain and the Omicron variant showed a non-monotonic dependence on protease expression levels. No synergy was observed at low and high protease expression levels, when virus entry through one of the two pathways was dominant (Fig. 5I, J). Synergy peaked at intermediate protease expression levels when the usage of the two entry pathways was comparable (Fig. 5I, J). Because the Omicron variant uses the TMRPSS2 pathway less efficiently and the Cathepsin B/L pathway more efficiently than the original strain, synergy for Omicron peaked at a relatively higher TMPRSS2 (Fig. 5I) and lower Cathepsin B/L (Fig. 5J) expression levels than for the original strain. Drug levels that would yield optimal synergy would thus be different for the original strain and the Omicron variant.

In summary, our model predicts that drug combinations targeting TMPRSS2 and Cathepsin B/L inhibitors would synergistically block original strain and Omicron variant entry, albeit to different extents in a protease expression level-dependent manner.

DISCUSSION

Recent studies have reported changes in cellular tropism and cell entry properties of the Omicron variant compared to the original SARS-CoV-2 strain and other variant (Garcia-Beltran et al., 2021; Hoffmann and et al, 2021; Meng et al., 2021; Peacock et al., 2022; Willett

et al., 2022; Zhao et al., 2021). Quantifying the changes in the preference of the Omicron variant for different entry routes may help evaluate the efficacies of entry inhibitors in clinical development and optimise entry inhibitor-based treatments (Gunst et al., 2021; Zhuravel et al., 2021). Mathematical models of SARS-CoV-2 kinetics have provided valuable insights into COVID-19 disease progression, drug action, and the effectiveness of vaccines and treatments (Amidei and Dobrovolny, 2022; Chatterjee et al., 2022; Desikan et al., 2021; Garg et al., 2021; Gonçalves et al., 2020; Goyal et al., 2020; Ke et al., 2021; Kissler et al., 2021; Néant et al., 2021; Padmanabhan et al., 2022; Perelson and Ke, 2020). Here, adapting a previously developed mathematical model of SARS-CoV-2 entry (Padmanabhan et al., 2020) to the analysis of *in vitro* data on variants (Garcia-Beltran et al., 2021; Hoffmann and et al, 2021), we quantified the altered usage of host proteases required for entry by the Omicron variant relative to the original strain and the Delta variant. We then applied the model to examine the influence of the latter on the efficacies and synergy of drugs targeting the host proteases mediating entry.

Our analysis suggests that the Omicron variant appears to have evolved to use Cathepsin B/L more efficiently and TMPRSS2 less efficiently than the original strain and the Delta variant for cell entry. Specifically, we estimated >4-fold enhanced efficiency in the usage of the Cathepsin B/L pathway and >3-fold reduced efficiency in the usage of the TMPRSS2 pathway by the Omicron variant in the cell lines examined. The alteration in the preference of the Omicron variant for entry pathways may have clinical implications. Drugs targeting TMPRSS2, such as camostat mesylate (Hoffmann et al., 2020a), and the Cathepsin B/L pathway, such as CA-074 methyl ester (Hashimoto et al., 2021), are in development. The efficacy of TMPRSS2 inhibitors is likely to decrease and that of Cathepsin B/L inhibitors is likely to increase against the Omicron strain. Our model predictions corroborated this expectation. Available experimental data too are consistent with this expectation. Camostat mesylate, a TMPRSS2 inhibitor, worked poorly against the Omicron variant compared to the

Delta variant in blocking infection *in vitro* (Zhao et al., 2021). Future studies may test whether Cathepsin B/L inhibitors would work better against the Omicron variant than the original and Delta strains. The mechanistic origins of the altered entry pathway usage by the Omicron variant remain poorly elucidated. Although molecular dynamics simulations can offer insights (Aggarwal et al., 2021; Ray et al., 2021; Zimmerman et al., 2021), the large number of mutations in the spike protein of the Omicron variant render the mechanisms difficult to unravel.

In a previous study, we predicted synergy between TMPRSS2 and Cathepsin B/L inhibitors against original SARS-CoV-2 infection (Padmanabhan et al., 2020). This synergy has since been observed experimentally (Hoffmann et al., 2020a; Kreutzberger et al., 2021). Here, we predicted that the drugs would also exhibit synergy against the Omicron variant. The extent of synergy and the drug concentrations at which the synergy would be maximum, however, are likely to be different for the Omicron variant compared to the other strains. The difference is expected because of the different entry pathway usages involved. Our formalism offers a route to identify the optimal drug concentrations using the distributions of the expression levels of the proteases and the dependent susceptibilities of cells to entry via the two pathways as inputs. While such inputs have been available for other viruses such as HIV-1 and hepatitis C virus and enabled quantitative model predictions (Brandenberg et al., 2015; Koizumi et al., 2017; Magnus et al., 2009; Mulampaka and Dixit, 2011; Padmanabhan and Dixit, 2011, 2015, 2017; Padmanabhan et al., 2014; Sen et al., 2019; Venugopal et al., 2018), they are currently not available for SARS-CoV-2. Consequently, our findings of drug efficacies and synergy, although robust, remain qualitative.

Since late 2021, more than a hundred Omicron sublineages, including BA.1.1, BA.2, BA.2.3, BA.2.75, BA.2.9, BA.2.12.1, BA.3, BA.4, and BA.5, have emerged (Xia et al., 2022). These sublineages have evolved to exhibit different transmissibility, virulence, and

414 immune evasion (Xia et al., 2022). Whether they also have different preferences for entry
415 routes is not fully understood. Our study has focussed on the BA.1 sublineage. Our model
416 presents a framework to analyse the emerging *in vitro* data and quantify the changes in the
417 entry pathways used by the other Omicron sublineages.

418 Implications of our findings also follow for our understanding of the cell tropism of the
419 Omicron variant. Because of its preferred and more efficient usage of the Cathepsin B/L
420 pathway, it is likely to preferentially infect cells expressing high levels of Cathepsin B/L. It
421 would be interesting to test whether such cells are present in greater abundance in the upper
422 respiratory tract, facilitating greater transmission of the Omicron variant than other pre-
423 Omicron variants. Similarly, future studies may test whether the reduced usage of TMPRSS2
424 results in less severe disease compared to the other variants.

425

426 **ACKNOWLEDGEMENTS**

427 We thank Rajat Desikan for help with Fig. 1A.

428

429 **COMPETING INTERESTS**

430 The authors declare that no conflicts of interests exist.

431

432 **REFERENCES**
433

434 Aggarwal, A., Naskar, S., Maroli, N., Gorai, B., Dixit, N.M., Maiti, P.K., 2021. Mechanistic
435 insights into the effects of key mutations on SARS-CoV-2 RBD-ACE2 binding. Phys Chem
436 Chem Phys 23, 26451-26458.

437 Amidei, A., Dobrovolny, H.M., 2022. Estimation of virus-mediated cell fusion rate of SARS-
438 CoV-2. Virology 575, 91-100.

439 Balistreri, G., Yamauchi, Y., Teesalu, T., 2021. A widespread viral entry mechanism: The C-
440 end Rule motif-neuropilin receptor interaction. Proc Natl Acad Sci U S A 118, e2112457118.

441 Brandenberg, O.F., Magnus, C., Regoes, R.R., Trkola, A., 2015. The HIV-1 entry process: A
442 stoichiometric view. Trends Microbiol 23, 763-774.

443 Cameroni, E., Bowen, J.E., Rosen, L.E., Saliba, C., Zepeda, S.K., Kulap, K., al., e., 2021.
444 Broadly neutralizing antibodies overcome SARS-CoV-2 Omicron antigenic shift. Nature 602,
445 664–670.

446 Chatterjee, B., Sandhu, H.S., Dixit, N.M., 2022. Modeling recapitulates the heterogeneous
447 outcomes of SARS-CoV-2 infection and quantifies the differences in the innate immune and
448 CD8 T-cell responses between patients experiencing mild and severe symptoms. PLoS Pathog
449 18, e1010630.

450 Desikan, R., Padmanabhan, P., Kierzek, A.M., van der Graaf, P.H., 2021. Mechanistic models
451 of COVID-19: Insights into disease progression, vaccines, and therapeutics. Int J Antimicrob
452 Agents 60, 106606.

453 Garcia-Beltran, W.F., Denis, K.J.S., Hoelzemer, A., Lam, E.C., Nitido, A.D., Sheehan, M.L.,
454 Berrios, C., al., e., 2021. mRNA-based COVID-19 vaccine boosters induce neutralizing
455 immunity against SARS-CoV-2 Omicron variant. Cell 185, 457-466.

456 Garg, A.K., Mittal, S., Padmanabhan, P., Desikan, R., Dixit, N.M., 2021. Increased B cell
457 selection stringency in germinal centers can explain improved COVID-19 vaccine efficacies
458 with low dose prime or delayed boost. Front Immunol 12, 776933.

459 Gonçalves, A., Bertrand, J., Ke, R., Comets, E., de Lamballerie, X., Malvy, D., Pizzorno, A.,
460 Terrier, O., Rosa Calatrava, M., Mentré, F., Smith, P., Perelson, A.S., Guedj, J., 2020. Timing
461 of antiviral treatment initiation is critical to reduce SARS-CoV-2 viral load. CPT:
462 Pharmacometrics Syst Pharmacol 9, 509-514.

463 Goyal, A., Cardozo-Ojeda, E.F., Schiffer, J.T., 2020. Potency and timing of antiviral therapy
464 as determinants of duration of SARS-CoV-2 shedding and intensity of inflammatory response.
465 Sci Adv 6, eabc7112.

466 Gunst, J.D., Staerke, N.B., Pahus, M.H., Kristensen, L.H., Bodilsen, J., Lohse, N., Dalgaard,
467 L.S., Brønnum, D., Fröbert, O., Hønge, B., Johansen, I.S., Monrad, I., Erikstrup, C., Rosendal,
468 R., Vilstrup, E., Mariager, T., Bove, D.G., Offersen, R., Shakar, S., Cajander, S., Jørgensen,
469 N.P., Sritharan, S.S., Breining, P., Jespersen, S., Mortensen, K.L., Jensen, M.L., Kolte, L.,
470 Frattari, G.S., Larsen, C.S., Storgaard, M., Nielsen, L.P., Tolstrup, M., Sædder, E.A.,
471 Østergaard, L.J., Ngo, H.T.T., Jensen, M.H., Højen, J.F., Kjolby, M., Søgaard, O.S., 2021.
472 Efficacy of the TMPRSS2 inhibitor camostat mesilate in patients hospitalized with Covid-19-
473 a double-blind randomized controlled trial. EClinicalMedicine 35, 100849.

474 Hashimoto, R., Sakamoto, A., Deguchi, S., Yi, R., Sano, E., Hotta, A., Takahashi, K.,
475 Yamanaka, S., Takayama, K., 2021. Dual inhibition of TMPRSS2 and Cathepsin B prevents
476 SARS-CoV-2 infection in iPS cells. Mol Ther Nucleic Acids 26, 1107-1114.

477 Hoffmann, M., et al, 2021. The Omicron variant is highly resistant against antibody-mediated
478 neutralization: Implications for control of the COVID-19 pandemic. Cell 185, 447-456.

479 Hoffmann, M., Kleine-Weber, H., Schroeder, S., Krüger, N., Herrler, T., Erichsen, S.,
480 Schiergens, T.S., Herrler, G., Wu, N.H., Nitsche, A., Müller, M.A., Drosten, C., Pöhlmann, S.,
481 2020a. SARS-CoV-2 cell entry depends on ACE2 and TMPRSS2 and is blocked by a clinically
482 proven protease inhibitor. Cell 181, 271-280.

483 Hoffmann, M., Schroeder, S., Kleine-Weber, H., Müller, M.A., Drosten, C., Pöhlmann, S.,
484 2020b. Nafamostat mesylate blocks activation of SARS-CoV-2: New treatment option for
485 COVID-19. Antimicrob Agents Chemother 64, e00754-00720.

486 Jackson, C.B., Farzan, M., Chen, B., Choe, H., 2022. Mechanisms of SARS-CoV-2 entry into
487 cells. Nat Rev Mol Cell Biol 23, 3-20.

488 Jiang, Y., van der Welle, J.E., Rubingh, O., van Eikenhorst, G., Bakker, W.A.M., Thomassen,
489 Y.E., 2019. Kinetic model for adherent Vero cell growth and poliovirus production in batch
490 bioreactors. Process Biochem 81, 156-164.

491 Ke, R., Zitzmann, C., Ho, D.D., Ribeiro, R.M., Perelson, A.S., 2021. In vivo kinetics of SARS-
492 CoV-2 infection and its relationship with a person's infectiousness. Proc Natl Acad Sci U S A
493 118, e2111477118.

494 Kissler, S.M., Fauver, J.R., Mack, C., Tai, C.G., Breban, M.I., Watkins, A.E., Samant, R.M.,
495 Anderson, D.J., Metti, J., Khullar, G., Baits, R., MacKay, M., Salgado, D., Baker, T., Dudley,
496 J.T., Mason, C.E., Ho, D.D., Grubaugh, N.D., Grad, Y.H., 2021. Viral dynamics of SARS-
497 CoV-2 variants in vaccinated and unvaccinated persons. N Engl J Med 385, 2489-2491.

498 Koch, J., Uckeley, Z.M., Doldan, P., Stanifer, M., Boulant, S., Lozach, P.Y., 2021. TMPRSS2
499 expression dictates the entry route used by SARS-CoV-2 to infect host cells. EMBO J 40,
500 e107821.

501 Koizumi, Y., Ohashi, H., Nakajima, S., Tanaka, Y., Wakita, T., Perelson, A.S., Iwami, S.,
502 Watashi, K., 2017. Quantifying antiviral activity optimizes drug combinations against hepatitis
503 C virus infection. Proc Natl Acad Sci U S A 114, 1922-1927.

504 Kreutzberger, A.J.B., Sanyal, A., Ojha, R., Pyle, J.D., Vapalahti, O., Balistreri, G.,
505 Kirchhausen, T., 2021. Synergistic block of SARS-CoV-2 infection by combined drug
506 inhibition of the host entry factors PIKfyve kinase and TMPRSS2 protease. J Virol 95,
507 e0097521.

508 Liu, J., Li, Y., Liu, Q., Yao, Q., Wang, X., Zhang, H., Chen, R., Ren, L., Min, J., Deng, F.,
509 Yan, B., Liu, L., Hu, Z., Wang, M., Zhou, Y., 2021. SARS-CoV-2 cell tropism and multiorgan
510 infection. Cell Discov 7, 17.

511 Magnus, C., Rusert, P., Bonhoeffer, S., Trkola, A., Regoes, R.R., 2009. Estimating the
512 stoichiometry of human immunodeficiency virus entry. J Virol 83, 1523-1531.

513 Meng, B., Ferreira, I.A.T.M., Abdullahi, A., Saito, A., Kimura, I., al., e., 2021. Altered
514 TMPRSS2 usage by SARS-CoV-2 Omicron impacts infectivity and fusogenicity. Nature 603,
515 706-714.

516 Mulampaka, S.N., Dixit, N.M., 2011. Estimating the threshold surface density of Gp120-CCR5
517 complexes necessary for HIV-1 envelope-mediated cell-cell fusion. PLoS One 6, e19941.

518 Néant, N., Lingas, G., Le Hingrat, Q., Ghosn, J., Engelmann, I., Lepiller, Q., Gaymard, A.,
519 Ferré, V., Hartard, C., Plantier, J.C., Thibault, V., Marlet, J., Montes, B., Bouiller, K., Lescure,
520 F.X., Timsit, J.F., Faure, E., Poissy, J., Chidiac, C., Raffi, F., Kimmoun, A., Etienne, M.,
521 Richard, J.C., Tattevin, P., Garot, D., Le Moing, V., Bachelet, D., Tardivon, C., Duval, X.,
522 Yazdanpanah, Y., Mentré, F., Laouénan, C., Visseaux, B., Guedj, J., 2021. Modeling SARS-

523 CoV-2 viral kinetics and association with mortality in hospitalized patients from the French
524 COVID cohort. Proc Natl Acad Sci U S A 118, e2017962118.

525 Ou, T., Mou, H., Zhang, L., Ojha, A., Choe, H., Farzan, M., 2021. Hydroxychloroquine-
526 mediated inhibition of SARS-CoV-2 entry is attenuated by TMPRSS2. PLoS Pathog 17,
527 e1009212.

528 Padmanabhan, P., Desikan, R., Dixit, N.M., 2020. Targeting TMPRSS2 and Cathepsin B/L
529 together may be synergistic against SARS-CoV-2 infection. PLoS Comput Biol 16, e1008461.

530 Padmanabhan, P., Desikan, R., Dixit, N.M., 2022. Modeling how antibody responses may
531 determine the efficacy of COVID-19 vaccines. Nat Comput Sci 2, 123-131.

532 Padmanabhan, P., Dixit, N.M., 2011. Mathematical model of viral kinetics in vitro estimates
533 the number of E2-CD81 complexes necessary for hepatitis C virus entry. PLoS Comput Biol
534 7, e1002307.

535 Padmanabhan, P., Dixit, N.M., 2012. Viral kinetics suggests a reconciliation of the disparate
536 observations of the modulation of claudin-1 expression on cells exposed to hepatitis C virus.
537 PLoS One 7, e36107.

538 Padmanabhan, P., Dixit, N.M., 2015. Modeling suggests a mechanism of synergy between
539 hepatitis C virus entry inhibitors and drugs of other classes. CPT Pharmacometrics Syst
540 Pharmacol 4, 445-453.

541 Padmanabhan, P., Dixit, N.M., 2017. Inhibitors of hepatitis C virus entry may be potent
542 ingredients of optimal drug combinations. Proc Natl Acad Sci U S A 114, E4524-E4526.

543 Padmanabhan, P., Garaigorta, U., Dixit, N.M., 2014. Emergent properties of the interferon-
544 signalling network may underlie the success of hepatitis C treatment. Nature Commun 5, 3872.

545 Peacock, T.P., Brown, J.C., Zhou, J., Thakur, N., Sukhova, K., Newman, J., Kugathasan, R.,
546 Yan, A.W., Furnon, W., De Lorenzo, G., 2022. The altered entry pathway and antigenic
547 distance of the SARS-CoV-2 Omicron variant map to separate domains of spike protein.
548 bioRxiv.

549 Perelson, A.S., Ke, R., 2020. Mechanistic modeling of SARS-CoV-2 and other infectious
550 diseases and the effects of therapeutics. Clin Pharmacol Ther, 10.1002/cpt.2160.

551 Ray, D., Le, L., Andricioaei, I., 2021. Distant residues modulate conformational opening in
552 SARS-CoV-2 spike protein. Proc Natl Acad Sci U S A 118, e2100943118.

553 Sen, P., Saha, A., Dixit, N.M., 2019. You cannot have your synergy and efficacy too. Trends
554 Pharmacol Sci 40, 811-817.

555 Ursache, R.V., Thomassen, Y.E., van Eikenhorst, G., Verheijen, P.J., Bakker, W.A., 2015.
556 Mathematical model of adherent Vero cell growth and poliovirus production in animal
557 component free medium. Bioprocess Biosyst Eng 38, 543-555.

558 Venugopal, V., Padmanabhan, P., Raja, R., Dixit, N.M., 2018. Modelling how responsiveness
559 to interferon improves interferon-free treatment of hepatitis C virus infection. PLoS Comput
560 Biol 14, e1006335.

561 Willett, B.J., Grove, J., MacLean, O.A., Wilkie, C., De Lorenzo, G., Furnon, W., Cantoni, D.,
562 Scott, S., Logan, N., Ashraf, S., Manali, M., Szemiel, A., Cowton, V., Vink, E., Harvey, W.T.,
563 Davis, C., Asamaphan, P., Smollett, K., Tong, L., Orton, R., Hughes, J., Holland, P., Silva, V.,
564 Pascall, D.J., Puxty, K., da Silva Filipe, A., Yebra, G., Shaaban, S., Holden, M.T.G., Pinto,
565 R.M., Gunson, R., Templeton, K., Murcia, P.R., Patel, A.H., Klenerman, P., Dunachie, S.,
566 Haughney, J., Robertson, D.L., Palmarini, M., Ray, S., Thomson, E.C., 2022. SARS-CoV-2
567 Omicron is an immune escape variant with an altered cell entry pathway. Nat Microbiol 7,
568 1161-1179.

569 Xia, S., Wang, L., Zhu, Y., Lu, L., Jiang, S., 2022. Origin, virological features, immune evasion
570 and intervention of SARS-CoV-2 Omicron sublineages. Signal Transduct Target Ther 7, 241.

571 Zhao, H., Lu, L., Peng, Z., Chen, L.L., Meng, X., Zhang, C., Ip, J.D., Chan, W.M., Chu, A.W.,
572 Chan, K.H., Jin, D.Y., Chen, H., Yuen, K.Y., To, K.K., 2021. SARS-CoV-2 Omicron variant
573 shows less efficient replication and fusion activity when compared with delta variant in
574 TMPRSS2-expressed cells. Emerg Microbes Infect 11, 277-283.

575 Zhuravel, S.V., Khmelnitskiy, O.K., Burlaka, O.O., Gritsan, A.I., Goloshchekin, B.M., Kim,
576 S., Hong, K.Y., 2021. Nafamostat in hospitalized patients with moderate to severe COVID-19
577 pneumonia: a randomised Phase II clinical trial. EClinicalMedicine 41, 101169.

578 Zimmerman, M.I., Porter, J.R., Ward, M.D., Singh, S., Vithani, N., Meller, A., Mallimadugula,
579 U.L., Kuhn, C.E., Borowsky, J.H., Wiewiora, R.P., Hurley, M.F.D., Harbison, A.M., Fogarty,
580 C.A., Coffland, J.E., Fadda, E., Voelz, V.A., Chodera, J.D., Bowman, G.R., 2021. SARS-CoV-
581 2 simulations go exascale to predict dramatic spike opening and cryptic pockets across the
582 proteome. Nat Chem 13, 651-659.
583

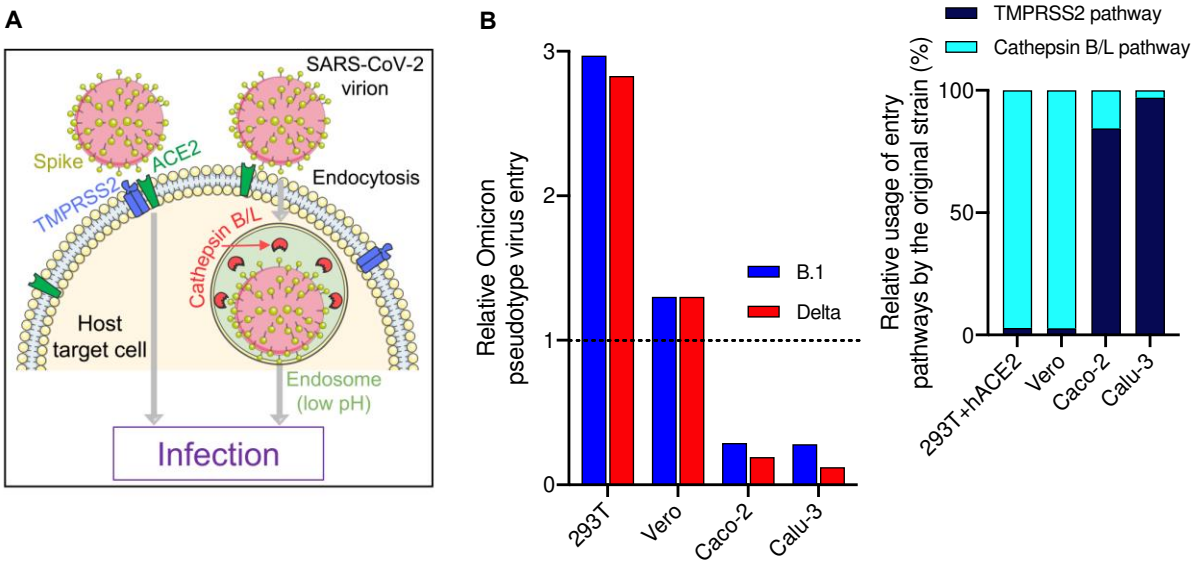

Figure 1. Omicron variant entry efficiency relative to B.1 and Delta strains correlates with the relative usage of the TMPRSS2 and Cathepsin B/L pathways. (A) Schematic of the two independent entry pathways accessible to SARS-CoV-2. **(B)** The Omicron entry efficiency relative to either the B.1 (blue) or the Delta (red) variant across cell types. Data was taken from Hoffmann et al. (2021). *Inset*, the relative usage of the entry pathways by the original strain. Data was taken from Padmanabhan et al. (2020).

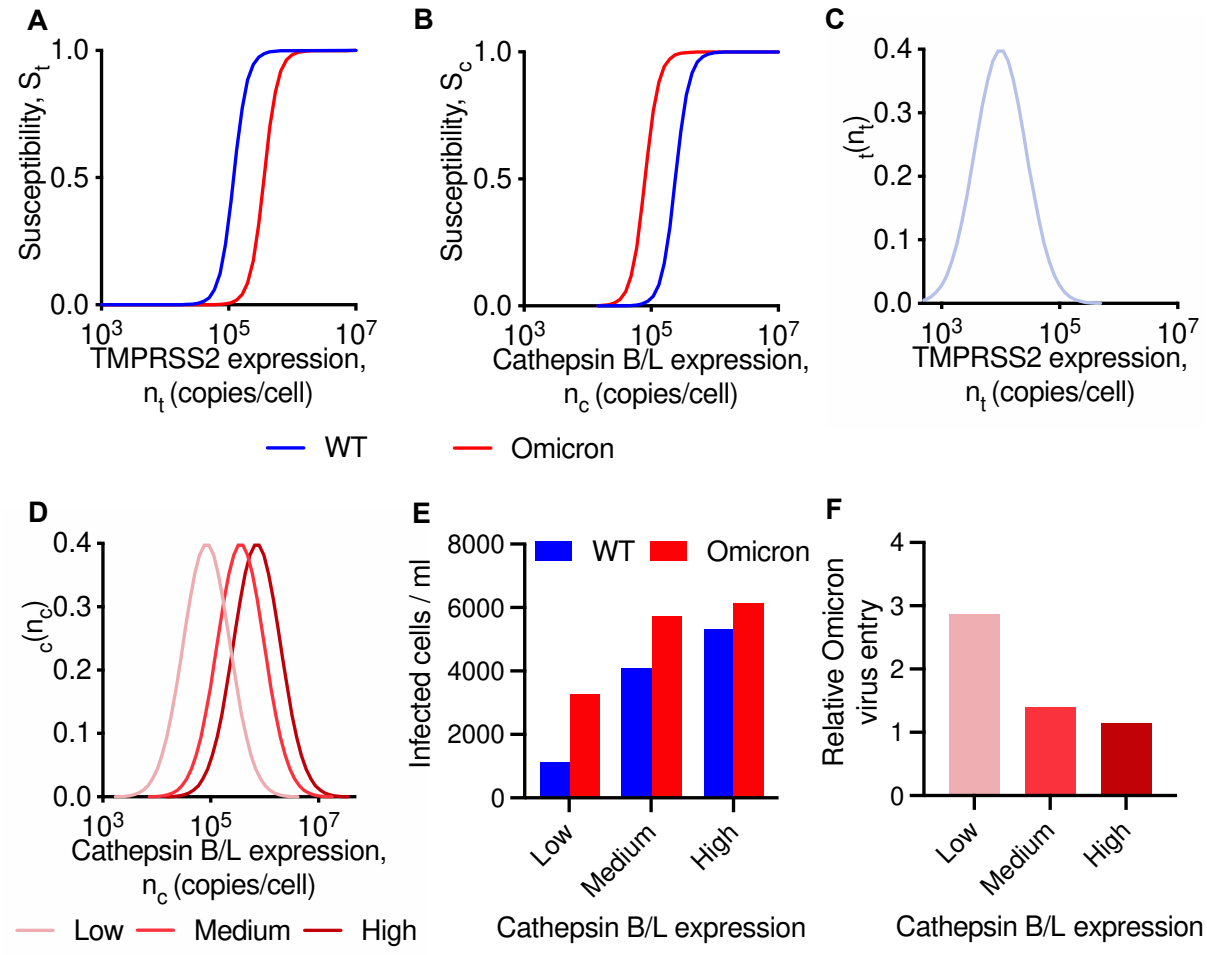

Figure 2. The relative entry efficiency of the Omicron variant depends on the protease expression. **(A, B)** Dependence of susceptibility of infection on TMPRSS2 (A) and Cathepsin B/L (B) expression levels for the original strain (blue line) and Omicron variant (red line). **(C)** The log-normal distribution of TMPRSS2 across cells with the mean TMPRSS2 expression levels $\overline{n_t}$ = 9.21. **(D)** The log-normal distribution of Cathepsin B/L across cells with low ($\overline{n_c}$ = 11.34), medium ($\overline{n_c}$ = 12.79) and high ($\overline{n_c}$ = 13.49) mean Cathepsin B/L expression levels. **(E, F)** Cells infected by the wild-type (blue bar) and Omicron variant (red bar) (E) and the Omicron entry efficiency relative to the original strain (F) at different Cathepsin B/L expression levels shown in Fig. 2D and fixed TMPRSS2 expression level shown in Fig. 2C. The other parameters and initial conditions are listed in Table 1.

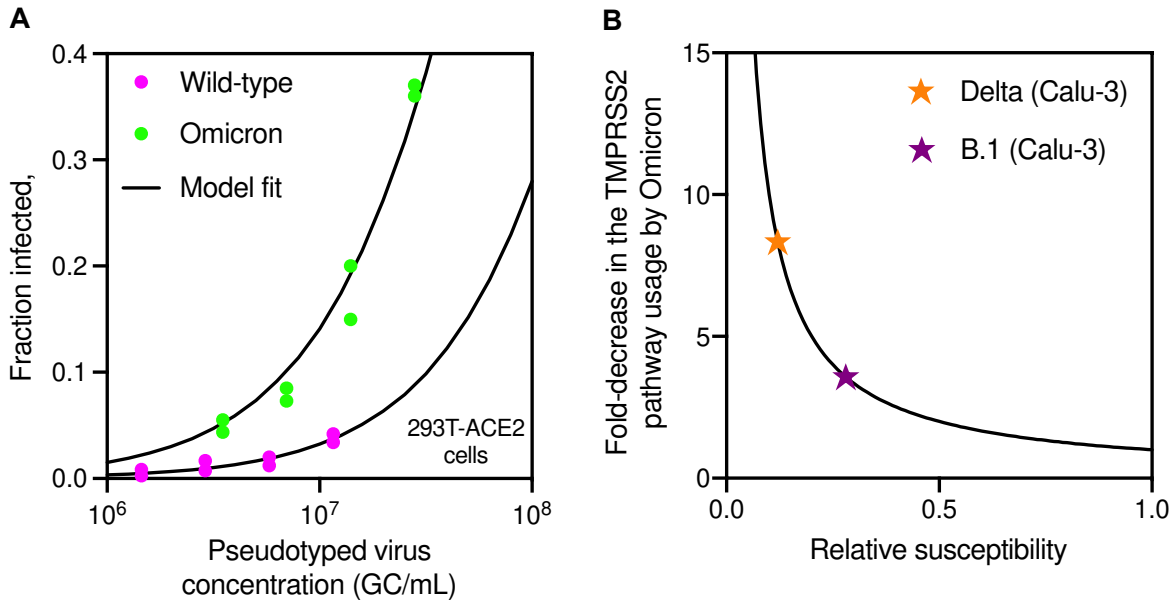

Figure 3. Estimation of entry pathway usage by the Omicron variant. **(A)** Fits of model predictions (lines) to the experimental data (symbols) taken from Garcia-Beltran et al. (2021) measuring the fraction of cells infected by pseudotyped virus bearing either the wild-type or the Omicron spike proteins. Data was fit using the tool NLINFIT in MATLAB R2017b. **(B)** The fold-decrease in Omicron entry efficiency through the TMPRSS2 pathway as a function of relative susceptibility to entry. Symbols place experimental data of relative infection taken from Hoffmann et al. (2021) on the relative susceptibility curve predicted (see text) so that the fold decrease can be read off. In A and B, experimental data was extracted using Engauge Digitizer 12.1.

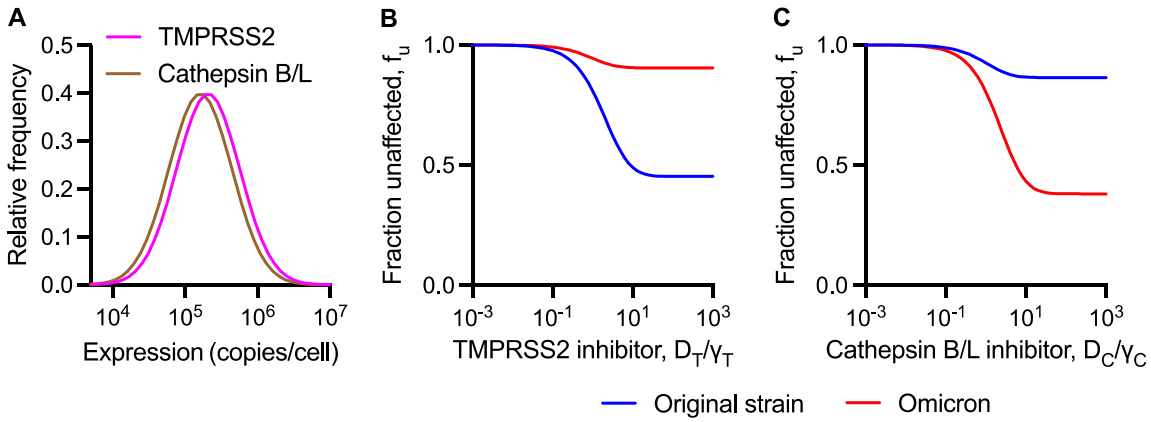

616

617 **Figure 4. Predictions of the efficacies of TMPRSS2 and Cathepsin B/L inhibitors against**
618 **the wild-type and Omicron variant. (A)** The log-normal distribution of TMPRSS2 and
619 cathepsin B/L across cells. **(B, C)** The fraction of infection events caused by the original strain
620 (blue line) and Omicron variant (red line) uninhibited by different concentrations of a
621 TMPRSS2 inhibitor (B) and a Cathepsin B/L inhibitor (C). In A-C, $\overline{n_c}$ = 12 and $\overline{n_t}$ = 12.25.
622 In D-E, $\overline{n_c}$ = 12. In F-G, $\overline{n_t}$ = 12.25. The other parameters and initial conditions are listed in
623 Table 1.
624
625
626

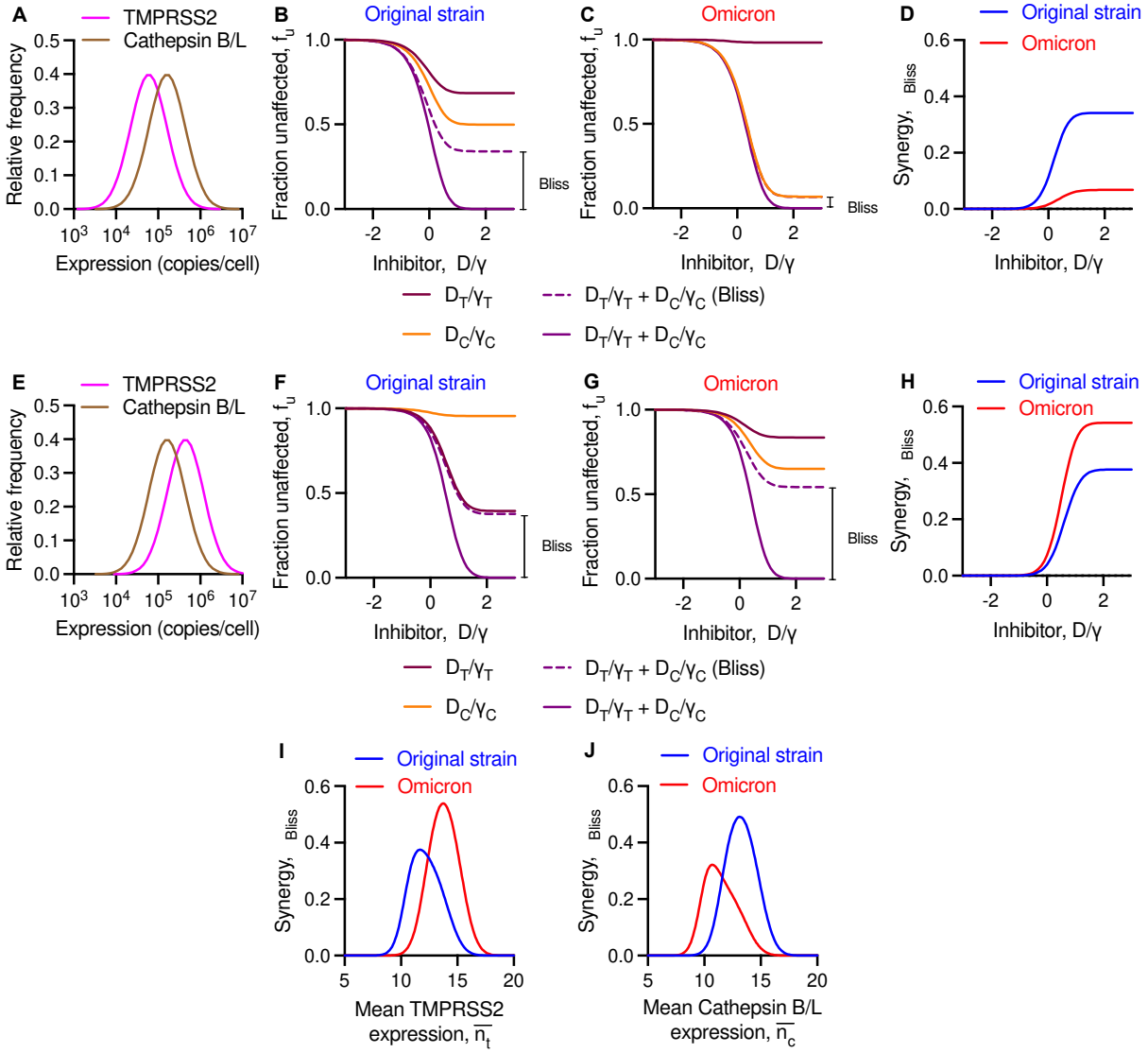

627

628 **Figure 5. Predictions of the effect of combination treatment targeting both TMPRSS2**
629 **and Cathepsin B/L pathways against the original strain and Omicron variant. (A-D)** The
630 log-normal distribution of TMPRSS2 and cathepsin B/L across cells (A) employed to predict
631 the fraction of infection events caused by the original strain (B) and the Omicron variant (C)
632 unaffected by Cathepsin B/L inhibitor, TMPRSS2 inhibitor or both and the Bliss synergy (D)
633 over a range of drug concentrations. **(E-H)** The log-normal distribution of TMPRSS2 and
634 cathepsin B/L across cells (E) employed to predict the fraction of infection events caused by
635 the original strain (F) and the Omicron variant (G) unaffected by Cathepsin B/L inhibitor,
636 TMPRSS2 inhibitor or both and the Bliss synergy (H) over a range of drug concentrations. In
637 B, C, F, and G, the extent of Bliss synergy is marked. **(I, J)** The predicted Bliss synergy for
638 varying TMPRSS2 expression and fixed mean ($\overline{n_c}$ = 12) Cathepsin B/L expression and for
639 varying Cathepsin B/L expression and fixed mean ($\overline{n_t}$ = 12) TMPRSS2 expression at two
640 different drug concentrations. In B-D and F-H, $D_C/\gamma_C = D_T/\gamma_T = D/\gamma$. In I, $\overline{n_c}$ = 12. In J, $\overline{n_t}$ =
641 12. In I-J, $D_C/\gamma_C = D_T/\gamma_T = 10$. The other parameters and initial conditions are listed in Table 1.
642
643

644 **Table 1: Model parameters and their values.**

Parameter	*Description*	*Values*	*Ref.*
λ	Target cell proliferation rate constant	0.77 d^{-1}	(Jiang et al., 2019)
μ	Target cell death rate constant	0.22 d^{-1}	(Ursache et al., 2015)
δ	Infected cell death rate constant	0.53 d^{-1}	(Gonçalves et al., 2020)
c_V	Virion clearance rate constant	10 d^{-1}	(Gonçalves et al., 2020)
k	Infection rate constant of cells with excess proteases	$1x10^{-4}$ ml ffu^{-1} d^{-1}	(Padmanabhan and Dixit, 2015)
$T(0)$	Initial target cells	$1x10^5$ cell ml^{-1}	(Padmanabhan and Dixit, 2015)
$V(0)$	Initial viral titre	$1x10^4$ ffu ml^{-1}	(Padmanabhan and Dixit, 2015)
t_d	Time of assessment	24 h	(Hoffmann et al., 2020a)
h_t	Hill coefficient	4	(Padmanabhan and Dixit, 2015)
h_c	Hill coefficient	4	(Padmanabhan and Dixit, 2015)
$\overline{n_t}$	Mean of TMPRSS2 distribution	6 – 18	Varied
$\overline{n_c}$	Mean of Cathepsin B/L distribution	6 – 18	Varied
n_t^{50} (Original strain)	TMPRSS2 expression at which $S_t = 0.5$	1.2 x 10^5 copies/cell	Assumed
n_c^{50} (Original strain)	Cathepsin B/L expression at which $S_c = 0.5$	2.4 x 10^5 copies/cell	Assumed
n_t^{50} (Omicron variant)	TMPRSS2 expression at which $S_t = 0.5$	3.6 x 10^5 copies/cell	Assumed
n_c^{50} (Omicron variant)	Cathepsin B/L expression at which $S_c = 0.5$	8 x 10^4 copies/cell	Assumed
σ_t	Standard deviation of TMPRSS2 distribution	1	(Padmanabhan and Dixit, 2015)
σ_c	Standard deviation of Cathepsin B/L distribution	1	(Padmanabhan and Dixit, 2015)

645 *ffu stands for focus-forming units. We set $p = 0$ for pseudoviruses.